

Article

# Strip Casting of Sm<sub>2</sub>TM<sub>17</sub>-Type Alloys for Production of the Metastable SmTM<sub>7</sub> Phase

Richard Sheridan \* , Joseph Gresle-Farthing, Alice Appleby and Mangaliso Brown

School of Metallurgy and Materials, University of Birmingham, Edgbaston, Birmingham B15 2TT, UK; j.greslefarthing@bham.ac.uk (J.G.-F.); axa1291@bham.ac.uk (A.A.); m.brown.4@bham.ac.uk (M.B.)

\* Correspondence: r.sheridan.1@bham.ac.uk

**Abstract:** Conventional book casting of Sm<sub>2</sub>TM<sub>17</sub>-type alloys (where TM = Co, Fe, Cu, Zr) leads to a coarse, highly segregated microstructure, predominantly due to the slow, variable cooling rate from the mould surface towards the centre of the ingot. These cast alloys require a long homogenisation treatment to remove this segregation and develop a super-saturated, metastable SmTM<sub>7</sub>-type hexagonal phase. This SmTM<sub>7</sub> phase is a vital precursor phase required during magnet production to develop the complex cellular structure responsible for high magnetic properties. In this work, strip casting was employed to facilitate rapid solidification to develop thin flakes (<0.5 mm thick) with a columnar grain structure. Rapid cooling has the potential to produce a homogenous microstructure consisting predominantly of the metastable SmTM<sub>7</sub> phase. This could remove or significantly reduce the need for the energy-intensive homogenisation treatment usually required in conventional magnet manufacture. This paper investigates the effect of wheel speed (and hence cooling rate) on flake thickness, microstructure, and phase balance of the cast alloys. It was shown that for wheel speeds between 1.1 and 3.0 m/s, the microstructure showed large variation; however, in all cases, evidence of the columnar SmTM<sub>7</sub> phase was presented. The adhesion between the melt and the wheel was deemed to be critical for the nucleation and subsequent columnar growth of SmTM<sub>7</sub> grains, where the wheel speed controlled both the flow of the alloy onto the wheel and the thickness of the resultant flake. It was determined that in order to achieve a homogenous columnar SmTM<sub>7</sub> structure, the maximum flake thickness should be limited to 270 µm to avoid the formation of equiaxed Sm<sub>2</sub>TM<sub>17</sub> grains through insufficient cooling.



**Citation:** Sheridan, R.; Gresle-Farthing, J.; Appleby, A.; Brown, M. Strip Casting of Sm<sub>2</sub>TM<sub>17</sub>-Type Alloys for Production of the Metastable SmTM<sub>7</sub> Phase. *Metals* **2024**, *14*, 517. <https://doi.org/10.3390/met14050517>

Academic Editor: Wenchao Yang

Received: 26 March 2024

Revised: 21 April 2024

Accepted: 25 April 2024

Published: 29 April 2024



**Copyright:** © 2024 by the authors. Licensee MDPI, Basel, Switzerland. This article is an open access article distributed under the terms and conditions of the Creative Commons Attribution (CC BY) license (<https://creativecommons.org/licenses/by/4.0/>).

**Keywords:** samarium cobalt; strip casting; metastable; rapid solidification

## 1. Introduction

Samarium cobalt (SmCo) magnets are high energy density permanent magnets suitable for applications such as high-speed motors and capable of operating at temperatures up to 550 °C. This is due to their excellent magnetic thermal coefficients, high Curie temperature, and a protective oxide (Sm<sub>2</sub>O<sub>3</sub>) layer, making them ideal for extreme environments [1]. One type of SmCo magnet is the 2:17 type, often referred to as Sm<sub>2</sub>TM<sub>17</sub>, where TM stands for transition metals (Co, Fe, Cu, Zr). The name 2:17 refers to the atomic ratio of Sm to transition metals in the hard-magnetic matrix phase. This nomenclature, as well as a capital letter denoting the crystal structure, will be used to refer to phases throughout this paper (see Table 1).

Sm<sub>2</sub>TM<sub>17</sub> magnets are highly dependent on a very particular phase structure, chemical composition, and heat treatment regime utilised during the manufacturing process [2]. This is a sub-granular nano-cellular microstructure that is comprised of FeCo-rich 2:17R rhombohedral Th<sub>2</sub>Ni<sub>17</sub>-type phase cells, providing the high energy product and remanence of the magnet [3]. These are surrounded by a Cu-rich boundary 1:5H hexagonal phase. The Cu concentration gradient between the cells and the boundary phase provides domain wall pinning, which is the dominant coercivity mechanism in 2:17 magnets [4]. A Zr-rich

phase forms a superimposed lamella and acts as a diffusion pathway during processing, allowing enrichment of the 2:17R cells with Fe and Co and the 1:5H boundary phase with Cu [5]. To form this structure,  $\text{Sm}_2\text{TM}_{17}$  magnets undergo long, high temperature heat treatments: firstly, a solution heat treatment at 1100–1200 °C for 4–10 h to form a metastable phase (1:7H), which is stabilised at room temperature by rapid quenching. This phase is described as disordered 2:17 in some literature and adopts a  $\text{TbCu}_7$  structure [6,7] which decomposes during subsequent heat treatment to develop a uniform, optimum micro/nano-structure [8–10]. This is followed by ageing at 750–850 °C for up to 12 h which allows the precipitation of the fine 2:17R cells and the formation and enrichment of the boundary phase from the precursor 1:7H phase. Further ageing is achieved by slow cooling to 400 °C and holding for 2–10 h to finesse the nanostructure of the magnet [11]. It should be noted that times and temperatures vary between manufacturers depending on specific elemental composition, desired grain size, desired cellular structure, and target magnetic properties.

**Table 1.** Reference table for the terminology used in this paper to describe the phases present within the microstructure.

Phase	Sm:TM Ratio	Crystal Structure	Crystal Structure Type
1:7H	1:7	Hexagonal	$\text{TbCu}_7$
1:5H	1:5	Hexagonal	$\text{CaCu}_5$
2:17R	2:17	Rhombohedral	$\text{Th}_2\text{Ni}_{17}$
2:17H	2:17	Hexagonal	$\text{Th}_2\text{Zn}_{17}$

In traditional manufacturing routes, the alloy is cast into water-cooled steel/copper moulds, causing variable cooling rate during solidification. The edges experience an extremely high cooling rate which diminishes towards the centre of the ingot. The variation in cooling rate causes an extremely inhomogeneous microstructure, segregated with large fractions of undesirable phases. Furthermore, these alloys are difficult to process, requiring high-energy jaw crushing and milling to reduce the particle size significantly. The composition and microstructure remain inhomogeneous, and hence heat treatment is crucial to achieving the desired magnetic properties [12]. The macrosegregation within the alloy is characterised by large regions rich in Fe and Co, with the other regions becoming enriched with Sm and Cu. Small amounts of the desirable metastable 1:7H phase are present in cast ingots, at the edges where the cooling rate is highest [13]. Theoretically, if the material could be cast with a sufficiently high cooling rate, the homogenisation step of the heat treatment could be skipped to save energy and thus cost.

Strip casting is a technique used in the production of other rare earth magnets that allows for rapid non-equilibrium cooling, potentially producing more desirable microstructures [14–17]. Strip casting works by pouring the melt onto a spinning water-cooled copper wheel, allowing for rapid solidification at cooling rates of around  $10^4$  K/s and producing long, thin flakes of the alloy. The wheel rotation speed is directly proportional to the cooling rate of the alloy but inversely proportional to the thickness of the flake it produces. The flake thickness of the alloy is typically between 100 and 1000  $\mu\text{m}$  compared to ingots, which are typically  $>10$  mm [13,17]. Strip cast flakes generally have a microstructure that varies along the direction of solidification across the thickness of the flake. Where the alloy initially contacts the wheel, a nucleation zone of rapidly solidified alloy forms. From this zone, directional columnar growth begins, consisting of fine needle-like grains with widths of only a few microns. As they grow along the direction of cooling towards the free side, eventually the rate of cooling is not sufficient to sustain their directional growth, and they lose their orientation, with their tips acting as nucleation sites for more randomly oriented grains. These grains are still relatively fine; however, they coarsen towards the free side of the strip. Long, thin flakes could also give a significant advantage during crushing and

milling, potentially requiring lower energy techniques to reduce particle size for magnet manufacture due to the highly brittle nature of the flakes.

Strip casting of  $\text{Sm}_2\text{TM}_{17}$  has only been explored in a few published papers, with only one paper seeking to obtain the 1:7H phase directly. Liu et al. found that casting at a wheel speed of 5 m/s produced a homogenous 1:7H phase structure with superficial nanoscale grains [18]. However, this was performed using a melt spinner, which is not truly representative of strip casting. The melt is ejected from the crucible onto the wheel using high pressure gas, giving cooling rates up to  $10^6$  K/s and producing ribbons that are typically 20–50  $\mu\text{m}$  thick, compared to strip casting, where the alloy is gravity fed onto the wheel, leading to higher thicknesses. This work presented by Liu et al. led to non-directional growth as the cooling rate was too high to allow for columnar, directional growth along a cooling gradient, which is synonymous with strip casting [18]. Meng et al. also investigated strip casting of  $\text{Sm}(\text{CoFeCuZr})_z$  alloys for magnet manufacture but did not detail the strip casting method or parameters used [19]. They found that the fine grains developed formed the majority of the strip cast alloy and were very detrimental to the remanence and energy product of sintered magnets. When the strip cast alloy was milled, the grain size in these regions was smaller than the average particle size, which led to polycrystalline particles with poor alignment in the final magnet. Therefore, an alloy consisting of columnar grains would likely be more beneficial to magnet production than the fine, equiaxed grains produced in this work [19]. Yang et al. [20] investigated the effect of strip casting wheel speed as a part of a larger study on magnet manufacture. They found that slower wheel speeds were more conducive to forming a microstructure suitable for magnet manufacture; however, they were not aiming for direct production of the 1:7H phase and were completing the entire manufacturing route as would be used for cast ingots containing heavy elemental segregation. Whilst this showed very promising results from a magnetic point of view, it did not focus on direct production of the metastable 1:7H phase [20]. Yang et al. [21] investigated hydrogen decrepitation of strip cast alloys similar to those presented in [20]. However, the micrograph showing the full cross-section of the alloy showed a rough surface that solidified in contact with the wheel, with a small nucleation zone and predominantly non-directional or equiaxed growth. There was very little evidence of the characteristic columnar growth associated with strip casting. Zheng et al. [22] also investigated the hydrogen absorption of strip cast  $\text{Sm}_2\text{TM}_{17}$ -type alloys; however, in this work, there was no attempt to optimise the strip casting process. The authors produced  $\sim 300$   $\mu\text{m}$  thick flakes with some columnar growth, although there was a large amount of variation in the directionality of the columnar grains. However, they did report up to  $\sim 30$ – $32$  wt% 1:7H phase in their alloys, which shows great promise for the work presented in this paper [22].

These studies have shown that non-equilibrium casting has the potential for tailoring the microstructure to avoid the need for long term heat treatment. This project instead aims to investigate the viability of strip casting  $\text{Sm}_2\text{TM}_{17}$ -type alloys to circumvent energy intensive homogenisation heat treatment in the production of sintered magnets.

## 2. Materials and Methods

In this work, 4.5 kg of master ingots of the composition  $\text{Sm}_{26.6}\text{Co}_{\text{Bal}}\text{Fe}_{19.9}\text{Cu}_{4.4}\text{Zr}_{2.3}$  (wt%) were loaded into the induction furnace of the strip caster for each individual casting. The alloy was heated to 1380 °C under a partial pressure of argon (200 mbar). The water-cooled wheel was ground with P120 SiC grinding paper to provide surface texture for the alloy to grip the wheel during casting. All casting parameters were kept constant, with the exception of the wheel rotational speed, which was varied across three casting runs with the following wheel speeds: Run 1 was cast at 1.1 m/s, Run 2 was cast at 2.1 m/s, and Run 3 was cast at 3.0 m/s. A schematic representation of the strip caster is shown in Figure 1.

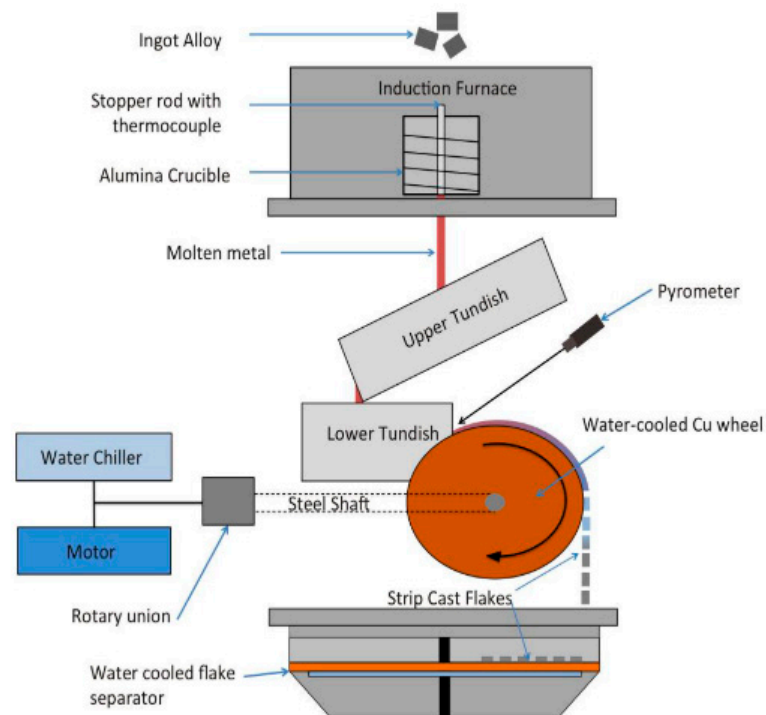


**Figure 1.** Labelled schematic of a pilot-scale strip caster at the University of Birmingham showing key components and flow of molten alloy from an induction furnace through a tundish system onto a water-cooled wheel to produce strip cast flakes, Adapted from Ref. [17].

Strip cast flake thickness measurements were taken using a digital micrometer, taking 100 measurements of randomly selected flakes to calculate the average flake thickness. The flakes were then broadly divided into three categories depending on thickness, and samples from each thickness range were mounted in cold setting epoxy resin for microscopy. These samples were ground using P800, P1200, P2400, and P4000 SiC grinding papers for 5 min per grit using an oil-based lubricant to prevent any reaction with water. Samples were subsequently polished using a 6  $\mu\text{m}$ , 1  $\mu\text{m}$ , and 0.25  $\mu\text{m}$  diamond compound in an oil based suspension for 10 min each using a Selvyt cloth. Scanning electron microscopy (SEM) was performed using a Hitachi 4000TMplus microscope (Tokyo, Japan) with an energy dispersive X-ray (EDX) detector in backscatter electron (BSE) mode with an accelerating voltage of 15 kV, a working distance of 9–11 mm, and magnification chosen to image the cross-section of the entire flake thickness for each sample. X-ray diffraction (XRD) was performed using Proto XRD with a  $2\theta$  range of 20–90° and a dwell time of 1 s.

### 3. Results

#### 3.1. As-Received Ingot

The as-received ingot was provided by Less Common Metals Ltd., Ellesmere Port, UK. The microstructure is shown in Figure 2 and demonstrates large areas of elemental segregation. The lighter regions (labelled B) were found to be rich in Sm and Cu, and the darker regions (labelled A) were rich in Co and Fe. XRD analysis identifies that the microstructure is predominantly the 2:17H phase with small amounts of 2:17R, 1:5H, and 1:7H phases present.

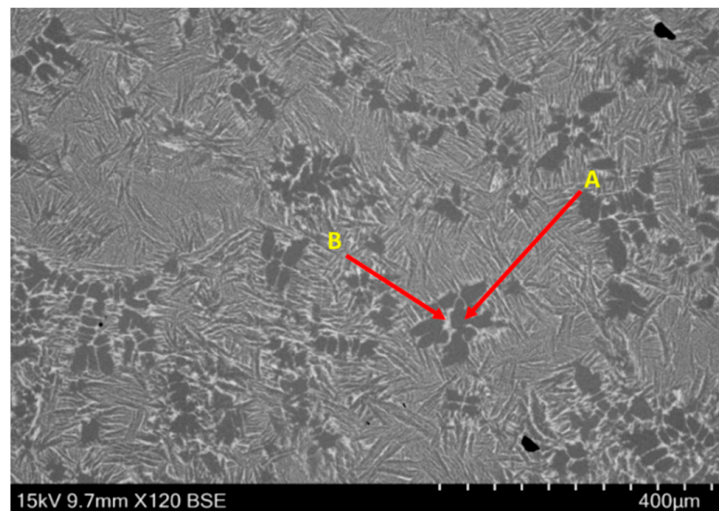


**Figure 2.** Microstructure of as-received ingot showing heavily segregated regions where label A represents a Co/Fe-rich phase and label B represents a Sm/Cu-rich phase.

### 3.2. Strip Cast Flakes

Thickness measurements for the three casting runs are shown in Figure 3. It was expected that as wheel speed increased, the flake thickness would decrease. This is because at higher wheel speeds, the alloy would be drawn onto the wheel more quickly and spread into thinner sheets. The mean flake thickness (and standard deviation) for Run 1 was 0.43 mm (0.06 mm), Run 2 was 0.45 mm (0.08 mm), and Run 3 was 0.40 mm (0.08 mm).

The microstructure of flakes taken from a variety of flake thicknesses from Runs 1–3 are shown in Figure 4. Each micrograph shows the entire cross-section of the flake, where the side directly in contact with the wheel during solidification is on the left and the top, free surface is on the right. The cooling direction is marked by a blue arrow. Each micrograph is accompanied by a coloured bar; the blue section indicates the nucleation zone where matrix grains are nucleated and columnar growth originates. The ideal microstructure would contain a short, uniform nucleation zone. The red zone indicates the region of columnar growth; this is where the cooling rate is optimal and is the ideal microstructure for further processing. The yellow section indicates the region where the cooling rate is too slow, columnar growth is no longer promoted, and non-directional grain growth occurs, along with elemental segregation, which requires heat treatment to remove. Quantification of each of these zones is presented in Table 2, where ranges of values are taken for each section as they are not completely uniform throughout the entire cross-section of the sample.

**Table 2.** Measurements of each microstructural zone within the samples selected from Runs 1, 2, and 3.

Sample	Nucleation Zone ( $\mu\text{m}$ )	Columnar Zone ( $\mu\text{m}$ )	Non-Direction Growth ( $\mu\text{m}$ )	Flake Thickness ( $\mu\text{m}$ )
Run 1 Thin	16	222–235	3–25	>252
Run 1 Median	Not Visible	102–140	245–267	>410
Run 1 Thick	17	112–179	236–275	>416
Run 2 Thin	19	225–251	26–46	>300
Run 2 Median	20	178–207	248–283	>457
Run 2 Thick	16	201	197	>418
Run 3 Thin	11	70–112	73–101	>201
Run 3 Median	7	53–90	216–280	>312
Run 3 Thick	Not Visible	52–68	311–350	>417

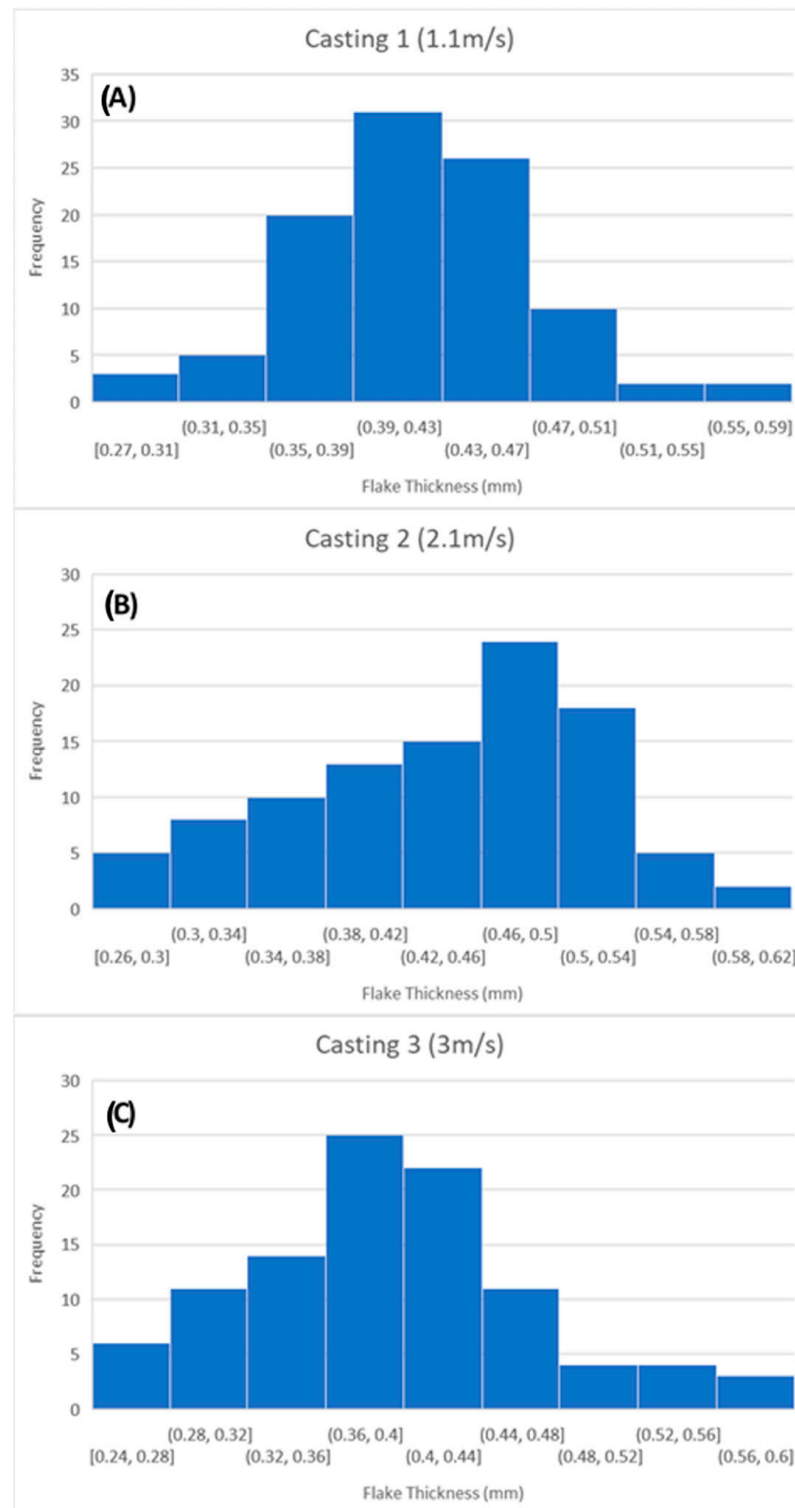


**Figure 3.** Flake thickness distributions from (A) Run 1, (B) Run 2, and (C) Run 3.

From Figure 4(A1), it can be seen that the thinnest flakes have a small nucleation region, a long region of columnar growth, and a small equiaxed region. The columnar grains are typically 1–2  $\mu\text{m}$  in width, opposite the central nucleation zone. The maximum length of this zone is 235  $\mu\text{m}$ , which reaches the free surface of the flake; however, the rest of the grains not directly in line with the nucleation zone become disoriented close to the free side of the flake. The median and thickest flakes (Figure 4(B1,C1), respectively), however, demonstrated very small regions of columnar growth (maximum length 140  $\mu\text{m}$

and 179  $\mu\text{m}$ , respectively) and predominantly consist of non-directional growth, with increased contrast in the image highlighting high levels of segregation observed in the median flake in particular. The phases that can be observed in these images are the 1:5H phase (white), the 1:7H phase (light grey), and the 2:17R/2:17H phases (dark grey).

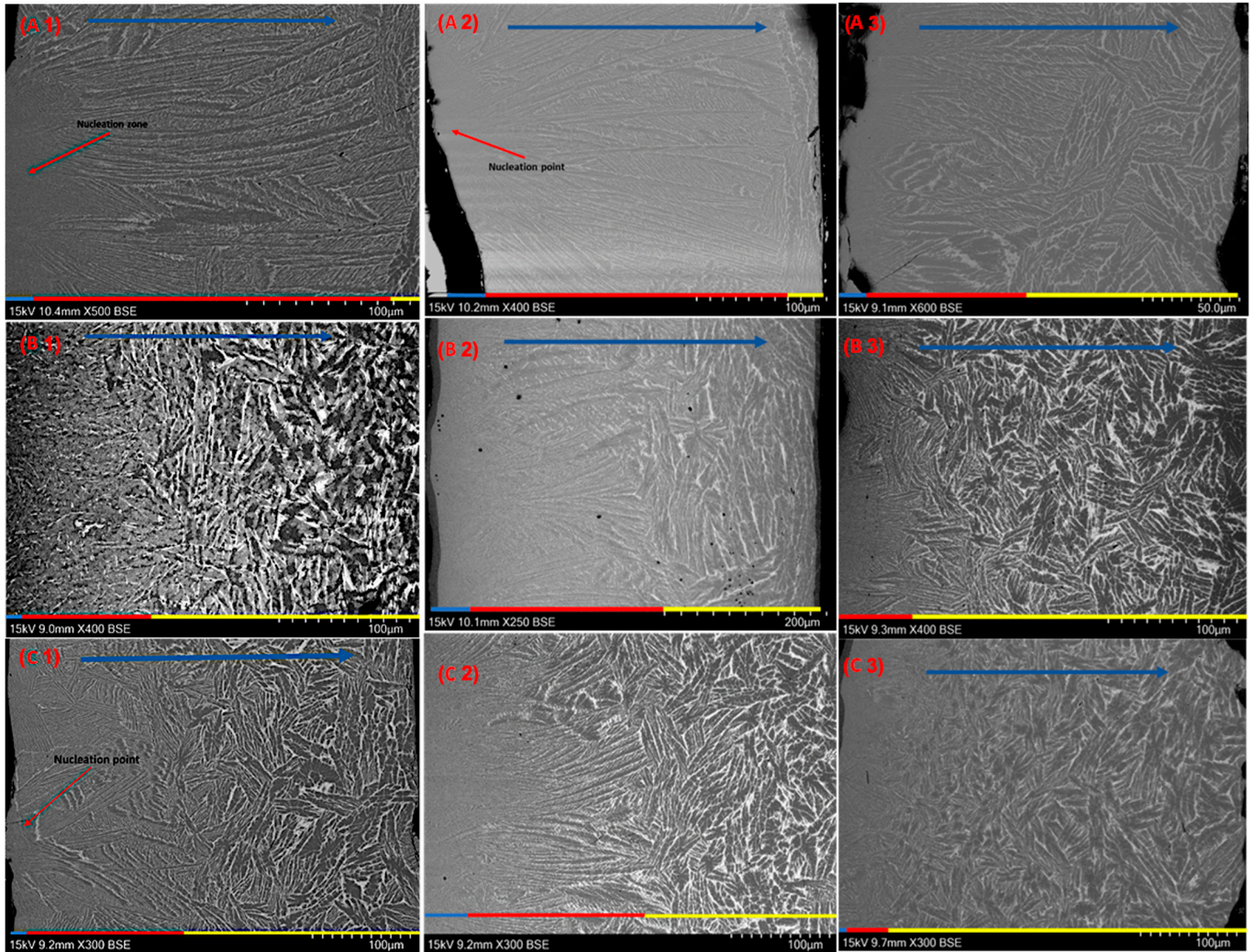


**Figure 4.** SEM micrographs of Run 1 from the (A1) thinnest, (B1) median, and (C1) thickest flakes; Run 2 from the (A2) thinnest, (B2) median, and (C2) thickest flakes; and Run 3 from the (A3) thinnest, (B3) median, and (C3) thickest flakes.

The microstructures of flakes from Run 2 show that the columnar growth regions in the median and thickest flakes (Figure 4(B2,C2), respectively) are longer than for Run 1 ( $\sim 207 \mu\text{m}$  and  $201 \mu\text{m}$ ). This was expected as the higher wheel speed should lead to a higher cooling rate, promoting columnar growth. The flake taken from the thinnest section, however, did not show a flat surface on the free side, where a single nucleation point could be identified, and all columnar growth emanated from this point with a maximum length of  $251 \mu\text{m}$ . This is likely to have occurred as a result of poor contact between the melt and the wheel during casting. It is highly likely that the molten alloy only contacted the wheel at this point on the first contact; it bounced/skipped and then gripped the wheel on the second contact. This means that initial solidification started on the first contact; the matrix phase nucleated and started growing, which was accelerated as the alloy made a second contact with the wheel. The non-directional region at the free side of the flake in this case is slightly larger ( $26\text{--}46 \mu\text{m}$ ) than in the thinnest flakes from Run 1 ( $3\text{--}25 \mu\text{m}$ ), due to the issues with contact with the wheel.

The microstructures of flakes from Run 3 are also shown in Figure 4. It can be seen that although the mean flake thickness was lower than in Runs 1 and 2 (see Figure 3), the microstructures are far from ideal. All three thicknesses show structures predominantly consisting of non-directional grains with very small regions of columnar growth. The thin flakes show a clear nucleation zone (Figure 4(A3)); however, it is less defined in the median and thickest flakes (Figure 4(B3,C3), respectively). This is likely due to poor adhesion/contact between the molten alloy and the wheel as it spins at high speed. The alloy is likely to have skipped or bounced off the wheel (as with the thinnest flake in Run 2); however, the contact in these cases was insufficient to maintain the required cooling rate for columnar growth, and the maximum length of columnar grains was just 112  $\mu\text{m}$ .

The microstructures of anomalies taken from Runs 1 and 2 are shown in Figure 5a,b, respectively. These flakes demonstrate the issues caused by the turbulent flow of the melt onto the wheel during strip casting. Figure 5a shows a flake where the thickness is not uniform; towards the top of the image, the flake is almost twice the thickness that it is at the bottom. In this case, there is a very typical nucleation zone on the wheel side, a columnar growth region, and then non-directional growth. Towards the top of the image, the microstructure would be deemed to have approximately equal columnar growth and non-directional growth, whereas in the thinner section, the microstructure is predominantly columnar growth with minimal non-directional growth.

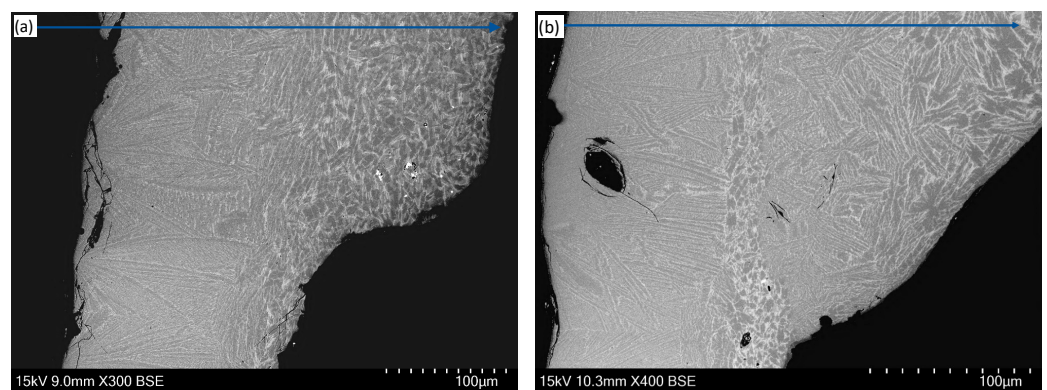


**Figure 5.** SEM micrographs of a non-uniform sample obtained from (a) Run 1 and (b) Run 2. The blue arrow indicates the cooling direction from the wheel side (a) to the free side (b).

In Figure 5b, the microstructure is much more irregular. It appears that a thin flake has initially been formed with a thickness of  $\sim 120 \mu\text{m}$  and a predominantly columnar structure. There is a large void within the flake, which was likely formed due to turbulence in the flow of the liquid onto the wheel. It appears from the micrograph that more liquid has flowed over the surface of the thin flake, which has created a band of highly segregated microstructure, likely due to re-melting of the top surface of the flake. The alloy that has flowed over the original flake has then solidified with some directional growth (left to right) and then non-directional growth towards the very right hand side of the image. This would suggest that as the secondary flow of melt solidified on a thin flake ( $\sim 120 \mu\text{m}$ ), the cooling rate was still sufficient to induce some level of columnar growth. It also gives further justification for the importance of controlling the flow of the alloy onto the wheel in order to obtain the desired microstructure.

Figure 6 shows XRD analysis of the as-received ingot as well as median flakes from each strip cast run, which was performed on coarse powders generated by grinding the flakes with a pestle and mortar. It can be seen that the traces of all strip cast runs are very different from the as-received ingot. The flakes from Run 1 show large fractions of 1:7H phase (denoted by \*) with small amounts of 1:5H and minor fractions of 2:17R. This shows that the cooling rate was largely sufficient to form 1:7H directly during strip casting, although evidence of the remaining minority phases highlights that the casting parameters were not quite ideal as some heat treatment would be required to develop the

1:7H metastable phase throughout the entire structure. Run 2 is very similar; however, there is evidence of an additional peak at  $48^\circ 2\theta$ , which corresponds to the presence of the 2:17H phase, which would be deleterious in further processing. Run 3 shows an increase in the phase fractions of 2:17R and 1:5H through increased peak intensity as well as the identification of new peaks for these phases.

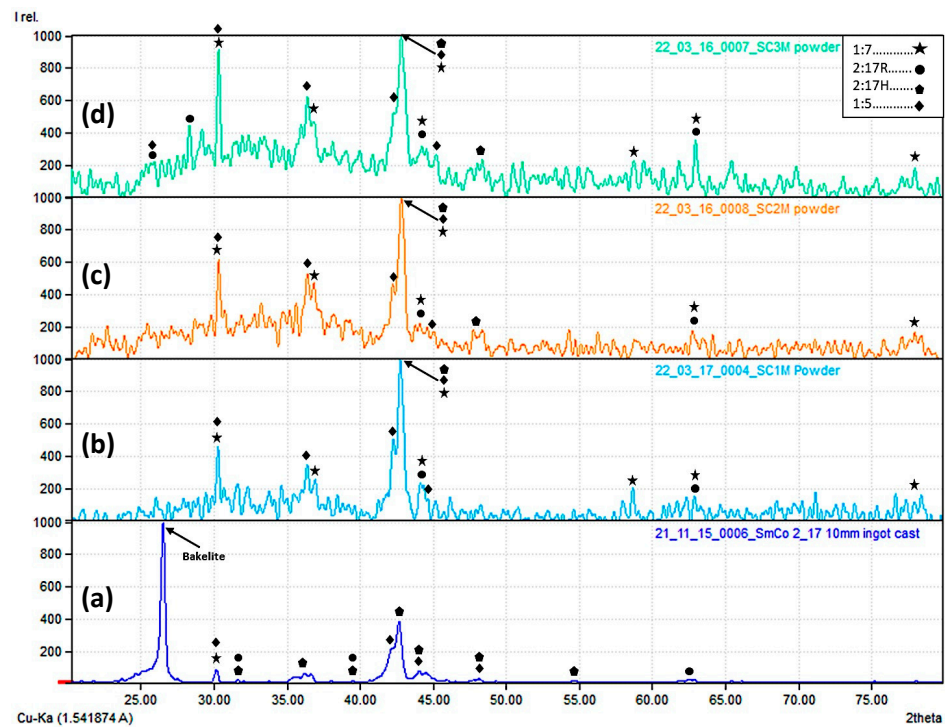


**Figure 6.** XRD traces for (a) as-received ingot and median flakes from (b) Run 1, (c) Run 2, and (d) Run 3.

XRD was also performed on the wheel side and free side of the complete flakes from the median batch from Run 1, as shown in Figure 7. These samples were also analysed using SEM and EDX to highlight the difference in microstructure on the flake surfaces and determine the compositional differences between the different phases, which are presented in Figure 8.

It can be seen that there is a significant difference in microstructure and phase balance between the as-received ingot, the wheel side of the flake, and the free side of the flake. This clearly indicates that there is a vast change in microstructure and phase balance as a result of strip casting. The change in microstructure through the cross section of the flake is also evident, as the peak locations and intensities vary from the wheel side to the free side of the flake. It was evident from the micrographs in Figure 4 that there were microstructural changes; however, the XRD analysis shows that this was not simply a change from columnar growth to equilibrium due to a change in cooling rate but also a change in phase balance as Sm and Cu rich phases are formed and segregate from the Fe and Co rich phases, which is evident from the BSE SEM images and EDX spectra in Figure 8. Interestingly, however, the XRD trace for the free side looks very different to that of the as-received ingot; this was partially due to a range of blue and gold coloured oxides being present on the surface as well as the fine, inhomogeneous microstructure. The peaks presented in Figure 7 do not accurately match those of the 1:5H, 1:7H, 2:17H, or 2:17R phases due to the surface oxides; hence, this data does not confirm the actual phase balance but clearly highlights a compositional difference between the two surfaces of the flakes. The EDX analysis shows that in general, the Sm and Cu content of the phases on the wheel side of the flake is higher than on the free side, and an inverse relationship is observed with Co and Fe.

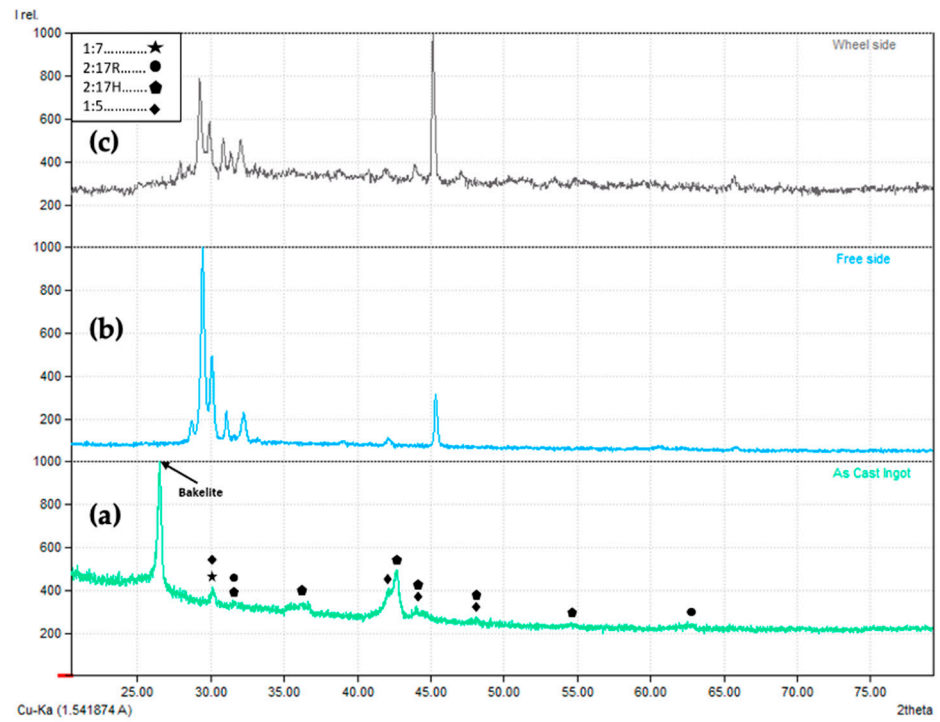
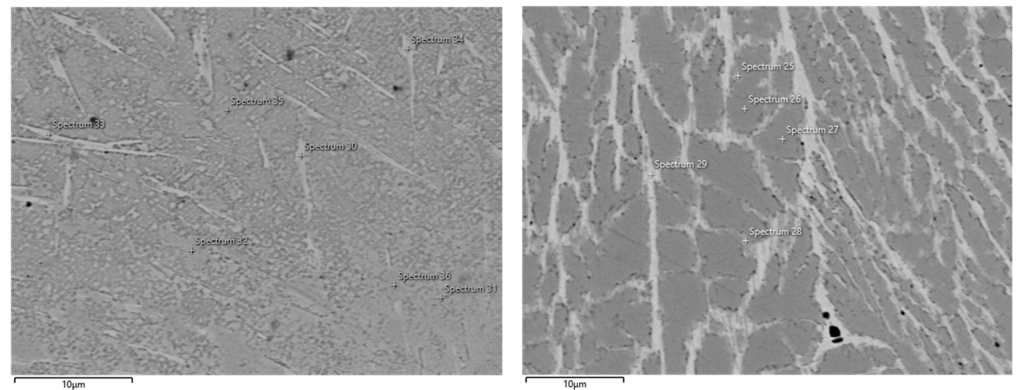


**Figure 7.** XRD traces for (a) the as-received ingot, (b) the free side, and (c) the wheel side of median flakes from Run 1.



	Sm (at%)	Co (at%)	Fe (at%)	Cu (at%)	Zr (at%)
<b>Wheel Side</b>					
Spectrum 30	15.71	53.84	18.00	7.34	5.12
Spectrum 31	12.74	53.03	23.80	8.72	1.70
Spectrum 32	12.21	53.71	24.85	6.28	2.48
Spectrum 33	10.05	51.24	24.89	11.79	1.51
Spectrum 35	12.92	52.42	21.74	10.08	2.85
Spectrum 36	12.75	53.09	24.42	7.70	1.53
<b>Free Side</b>					
Spectrum 25	7.02	54.37	23.76	13.01	1.36
Spectrum 27	10.90	55.27	27.97	4.67	1.18
Spectrum 28	11.69	54.80	26.87	4.80	1.63
Spectrum 29	14.47	54.65	20.90	6.81	3.17

**Figure 8.** BSE SEM images of the wheel side (left) and free side (right) of the median flake from Run 1, along with EDX spectra from the points highlighted on the micrographs.

#### 4. Discussion

The as-received cast alloys consist predominantly of the 2:17H phase with small amounts of the 2:17R, 1:5H, and 1:7H phases, and the microstructure demonstrated significant elemental segregation as a result of slow cooling in a water-cooled mould. The macrosegregation of Fe and Co to the dark phase and Cu and Sm to the light phase would require a homogenisation treatment to be removed before further processing into a magnet. For all strip cast alloys, however, the phase distribution changed substantially to consist predominantly of the metastable 1:7H phase with small amounts of 1:5H phase and trace 2:17R phase. Due to the substantially increased cooling rate, the microstructure typically consisted of a nucleation zone where the melt started to solidify in contact with the wheel and columnar growth along the thermal gradient from the wheel side of the flake towards the free side, similar to that demonstrated by Meng et al. [19] and Yang et al. [20]. However, in a number of flakes, there were regions where the cooling rate was not sufficient to maintain columnar growth, resulting in non-directional growth towards the free side of the flake and elemental segregation similar to that observed in the as-received cast alloy.

It was expected that as wheel speed increased, the flake thickness would be reduced as the molten alloy was pulled onto the wheel more quickly, which should result in thinner flakes consisting of columnar grains and the absence of non-directional growth. However, the faster wheel speed of 3.0 m/s produced a strip cast alloy with minimal columnar growth and predominantly non-directional growth and elemental segregation. Further analysis of Figure 4 showed that the contact surface between the wheel and the molten alloy was inconsistent as turbulence was introduced due to the high wheel speed. The sample that produced the most ideal microstructure was actually produced at the lowest wheel speed of 1.1 m/s in the thinnest flakes from the batch. The flake thickness was 252  $\mu\text{m}$ , demonstrating a uniform microstructure consisting of a nucleation zone 16  $\mu\text{m}$  thick, a columnar region of 222–235  $\mu\text{m}$ , and non-directional growth of 3–25  $\mu\text{m}$ . In terms of maximum columnar growth region, the thinnest flakes produced with a wheel speed of 2.1 m/s were 300  $\mu\text{m}$  thick, with a 19  $\mu\text{m}$  nucleation zone, 225–251  $\mu\text{m}$  columnar region, and 24–46  $\mu\text{m}$  non-directional growth. This would suggest that the maximum flake thickness should be 270  $\mu\text{m}$  thick to include the nucleation zone and columnar region whilst avoiding non-directional growth where the cooling rate cannot be sustained. Considering the microstructure across all samples suggests that control of the melt flowing onto the wheel and the contact surface between the melt and the wheel is more important for obtaining the desired microstructure than the rotational speed of the wheel. This was further highlighted by the microstructural anomalies presented in Figure 5, where turbulent flow led to inconsistent flake thickness and dual-microstructures within a flake. In a commercial system where >300 kg of alloy is produced in a single casting, small amounts of alloy with undesirable microstructures are unlikely to be detected and will be mixed in with the optimised material. However, in pilot-scale strip casters, there is more likely to be differential contact and cooling within a batch due to the low amount of alloy in the system (<5 kg) and sampling of the flakes for analysis after casting, resulting in a higher proportion of undesirable alloy. This has not been identified in most literature studies, as they utilise melt spinners that use pressurised gas to consistently eject the material onto the wheel rather than gravity feed through a series of tundishes. This is therefore not representative of commercial strip casting systems.

The XRD analysis presented in Figure 6 shows that the cooling rate was largely sufficient to form 1:7H directly during strip casting, although evidence of the remaining minority phases highlights that the casting parameters were not quite ideal as some heat treatment would be required to develop the 1:7H metastable phase throughout the entire structure. Figure 7 showed a difference in key peak intensities between the wheel side of the flake and the free side, which confirmed that the change in microstructure from the nucleation zone to the columnar region to non-directional growth is accompanied by a significant change in phase balance between the desired and detrimental phases. This was confirmed by the SEM and EDX analyses presented in Figure 8. Overall, this would suggest that further optimisation of the tundish design to better control alloy flow

onto the wheel would likely result in the desired columnar microstructure and phase balance of 1:7H and 1:5H without non-directional growth or unwanted minority phases. Alternatively, increasing the surface roughness of the wheel through shot blasting may increase adhesion between the wheel and the melt and result in more consistent cooling throughout the alloy.

When comparing these findings to those of Liu et al. [16] and Liu et al. [18], the flakes in this work show lower homogeneity in terms of phase balance and microstructure. Liu found that their strip cast ribbons contained the majority 1:7H phase with small traces of 1:5H, whereas this work found the majority 1:7H phase with fractions of 1:5H, 2:17H, and 2:17R. As Liu used the melt spinning technique to replicate strip casting, it is very likely that uniform contact was observed between the melt and the wheel as a result of the force applied by pressurised gas. This means that the cooling rate will be much more uniform than in gravity fed strip casting, as presented in this paper. However, homogeneity in the cooling rate means that the cross-sectional microstructure presented non-directional growth rather than columnar growth [16,18]. The fine-grained strip cast ribbons also led to lower remanence in fully processed magnets as it was not possible to produce single crystal particles by milling, which may not be a problem with the strip cast alloys presented in this work. Meng et al. [19] demonstrated strip cast flakes that were 575  $\mu\text{m}$  thick, where fine grains dominated 445  $\mu\text{m}$  of the thickness and columnar grains the remaining 130  $\mu\text{m}$ . This also led to a reduction in the magnetic properties of processed magnets compared to ingot starting materials, which was attributed to the high proportion of fine-grained material leading to polycrystalline particles after milling. As the strip casting parameters were not given and limited microstructural analysis was presented, no direct comparisons can be made regarding the optimisation of the strip casting process. Yang et al. and Yang et al. [20,21] demonstrated very similar findings to Meng et al. [19], showing that slower wheel speeds in strip casting led to better magnetic properties; however, as Meng et al., were utilising the full manufacturing route for magnet processing and were not aiming to circumvent the long heat treatment as would be the aim of this work. Likewise, direct comparison with Zheng et al. [22] is limited as they did not optimise the strip casting process; however, they obtained a similar combination of phases of the alloy but were not able to demonstrate directional columnar growth from the wheel side to the free side of the flake as presented in this work.

## 5. Conclusions

The work presented in this paper has shown that it is possible to produce Sm<sub>2</sub>Tm<sub>17</sub>-type alloys directly from strip casting to give a microstructure predominantly consisting of the SmTm<sub>7</sub> hexagonal phase. Lower wheel speeds of 1.1 m/s and 2.1 m/s yield alloys with a higher proportion of the 1:7H phase with a more homogenous structure, which was attributed to better adhesion between the molten alloy and the water-cooled wheel during solidification. A wheel speed of 3 m/s led to significant elemental segregation within the microstructure due to poor adhesion of the melt to the wheel during solidification. The highest length columnar growth region was found to be 251  $\mu\text{m}$ , consisting mainly of the 1:7H phase, which could be a maximum flake thickness to achieve a fully columnar structure. It was shown that controlling the contact between the melt and the wheel is more important than wheel speed alone to ensure that contact and cooling is sufficient throughout. Further optimisation of the process, for example, by changing tundish design and gate height to better control flow of the alloy onto the wheel or shot blasting the wheel to increase texture and hence aid gripping of the alloy to the wheel, could lead to fully homogenous 1:7H structures, removing the need for the homogenisation and solutionising stages of magnet production.

**Author Contributions:** Conceptualization, R.S.; Methodology, R.S., J.G.-F., A.A. and M.B.; Validation, A.A., J.G.-F. and M.B.; Formal Analysis, R.S. and J.G.-F.; Investigation, R.S., A.A., J.G.-F. and M.B.; Resources, R.S.; Writing—Original Draft Preparation, R.S. and J.G.-F.; Writing—Review and Editing, R.S., A.A., J.G.-F. and M.B.; Visualization, A.A. and J.G.-F.; Supervision, R.S.; Project Administration, R.S.; Funding Acquisition, R.S. All authors have read and agreed to the published version of the manuscript.

**Funding:** This research received no external funding.

**Data Availability Statement:** The raw data supporting the conclusions of this article will be made available by the authors on request.

**Acknowledgments:** The authors would like to acknowledge Less Common Metals Ltd. for supply of the master ingots used in this study.

**Conflicts of Interest:** The authors declare no conflicts of interest.

## References

1. Yi, J.-H. Development of samarium–cobalt rare earth permanent magnetic materials. *Rare Met.* **2014**, *33*, 633–640. [[CrossRef](#)]
2. Dormidontov, N.A.; Kolchugina, N.B.; Profol'ev, P.A.; Zheleznyi, M.V.; Milov, Y.V.; Dormidontov, A.G.; Bakulina, A.S. Structural constituents and phases in high-coercivity (Sm,Zr)(Co,Cu,Fe)<sub>z</sub> alloys for permanent magnets. *Russ. Metall.* **2022**, *2022*, 505–511. [[CrossRef](#)]
3. Hadjipanayis, G.C.; Tang, W.; Zhang, Y.; Chui, S.T.; Liu, J.F.; Chen, C. High temperature 2:17 magnets: Relationship of magnetic properties to microstructure and processing. *IEEE Trans. Magn.* **2000**, *36*, 3382–3387. [[CrossRef](#)]
4. Shang, Z.F.; Zhang, D.T.; Altounian, Z.; Xie, Z.H.; Qiao, P.B.; Liu, W.Q. Effect of ingot cooling rate on Cu distribution and magnetic properties of Sm(Co<sub>0.28</sub>Fe<sub>0.28</sub>Cu<sub>0.07</sub>Zr<sub>0.03</sub>)<sub>7.6</sub> magnets. *AIP Adv.* **2019**, *9*, 125–142. [[CrossRef](#)]
5. Shang, Z.; Zhang, D.; Xie, Z.; Wang, Y.; Haseeb, M.; Qiao, P. Effects of copper and zirconium contents on microstructure and magnetic properties of Sm(Co,Fe,Cu,Zr)<sub>z</sub> magnets with high iron content. *J. Rare Earths* **2021**, *39*, 160–166. [[CrossRef](#)]
6. Xue, Z.Q.; Liu, L.; Liu, Z.; Li, M.; Lee, D.; Chen, R.J. Mechanism of phase transformation in 2:17 type SmCo magnets investigated by phase stabilization. *Scr. Mater.* **2016**, *113*, 226–230. [[CrossRef](#)]
7. Yan, A.; Gutfleisch, O.; Handstein, A. Microstructure, microchemistry, and magnetic properties of melt-spun magnets. *J. Appl. Phys.* **2003**, *93*, 7975. [[CrossRef](#)]
8. Horiuchi, Y.; Hagiwara, M.; Okamoto, K.; Kobayashi, T.; Endo, M.; Kobayashi, T.; Nakamura, T.; Sakurada, N. Effects of solution treated temperature on the structural and magnetic properties of iron-rich Sm(Co,Fe,CuZr)<sub>z</sub> sintered magnet. *IEEE Trans. Magn.* **2013**, *49*, 3221–4224. [[CrossRef](#)]
9. Musa, M.; Zhou, X.; Song, X.; Yuan, T.; Jia, W.; Wang, J.; Ma, T. Fe content influence on the microstructure of solution-treated Sm-Co-Fe-Cu-Zr alloys. *Intermetallics* **2021**, *129*, 107049. [[CrossRef](#)]
10. Hu, M.; Kang, D.; Zhang, T.; Liu, B.; Xi, L.; Cao, J.; Xu, C.; Zuo, S.; He, Y.; Jiang, C. Single 1:7H solid-solution phase achieving in iron-rich Sm-Co-Fe-Cu-Zr magnets. *J. Alloys Compd.* **2023**, *945*, 169373. [[CrossRef](#)]
11. Cui, C.; Liu, X.; Nlebedim, C.I.; Cui, J. Mechanically strengthened heterogeneous Sm-Co sintered magnets. *J. Alloys Compd.* **2022**, *904*, 163937. [[CrossRef](#)]
12. Campbell, A. Investigations into the Optimisation of the Commercial Processing Route for Sm<sub>2</sub>Co<sub>17</sub> Type Permanent Magnets. Ph.D. Thesis, University of Birmingham, Birmingham, UK, 2018.
13. Appleby, A. Investigating the Viability of Strip Casting Samarium Cobalt 2:17. Master's Thesis, University of Birmingham, Birmingham, UK, 2021.
14. Zapuskalov, N. Comparison of Continuous Strip Casting with Conventional Technology. *ISIJ Int.* **2003**, *43*, 1115–1127. [[CrossRef](#)]
15. Pei, W.; He, C.; Lian, F.; Zhou, G.; Yang, H. Structures and magnetic properties of sintered Nd–Fe–B magnets produced by strip casting technique. *J. Magn. Magn. Mater.* **2002**, *239*, 475–478. [[CrossRef](#)]
16. Liu, Z.; Liu, L.; Chen, R.J.; Sun, Y.L.; Lee, D.; Yan, A.R. Optimization of temperature coefficient of remanence and magnetic properties of sintered Sm<sub>0.7</sub>Dy<sub>0.1</sub>Gd<sub>0.2</sub>(Co<sub>0.28</sub>Fe<sub>0.28</sub>Cu<sub>0.08</sub>Zr<sub>0.025</sub>)<sub>7.2</sub> magnets prepared by strip-casting technique. *IEEE Tran. Magn.* **2013**, *49*, 5599–5602. [[CrossRef](#)]
17. Meakin, J.P. Development of a pilot scale strip casting system to produce optimised alloys for neodymium-iron-boron magnets. Ph.D. Thesis, University of Birmingham, Birmingham, UK, 2015.
18. Liu, L.; Liu, Z.; Chen, R.; Liu, X.; Yan, A.; Lee, D.; Li, W. Effect of strip casting on microstructure and magnetic properties of 2:17 type Sm-Co sintered magnets. *IEEE Trans. Magn.* **2014**, *50*, 2101704. [[CrossRef](#)]
19. Meng, C.Z.; Zhang, D.T.; Jia, J.H.; Yang, J.J.; Teng, Y.; Zhang, H.G.; Li, Y.Q.; Liu, W.Q.; Yue, M. Effect of casting methods on magnetic properties of Sm(CoFeCuZr)<sub>z</sub> magnet. In Proceedings of the 67th Annual Conference on Magnetism and Magnetic Materials, Minneapolis, MN, USA, 31 October–4 November 2023; Volume 13.

20. Yang, Y.; Zhang, D.; Zhang, H.; Li, Y.; Meng, C.; Teng, Y.; Liu, W.; Yue, M. Combination strategy for high-performance Sm(CoFeCuZr)<sub>z</sub> sintered permanent magnet: Synergistic improvement of the preparation process. *Acta Mater.* **2023**, *251*, 118901. [[CrossRef](#)]
21. Yang, J.; Zhang, D.; Zhang, H.; Shang, Z.; Wang, H.; Meng, C.; Liu, W.; Yue, M. Effect of hydrogen pressure on hydrogenation and pulverization behaviour of Sm(CoFeCuZr)<sub>z</sub> ingot and strip casting flake. *J. Alloys Compd.* **2023**, *930*, 167427. [[CrossRef](#)]
22. Zheng, M.; Bi, Y.; Hou, Z.; Wang, C.; Wang, J.; Wang, L.; Duan, Z.; Zhang, B.; Fang, Y.; Zhu, M.; et al. Enhanced hydrogen adsorption capability of 2: 17-type Sm-Co strips via microstructure modification. *J. Alloys Compd.* **2024**, *987*, 174182. [[CrossRef](#)]

**Disclaimer/Publisher's Note:** The statements, opinions and data contained in all publications are solely those of the individual author(s) and contributor(s) and not of MDPI and/or the editor(s). MDPI and/or the editor(s) disclaim responsibility for any injury to people or property resulting from any ideas, methods, instructions or products referred to in the content.